Judith A. Simcox,[1] Thomas Creighton Mitchell,[2] Yan Gao,[1] Steven F. Just,[2] Robert Cooksey,[3] James Cox,[1] Richard Ajioka,[1] Deborah Jones,[2] Soh-hyun Lee,[2] Daniel King,[1] Jingyu Huang,[1]and Donald A. McClain[1,2,3]

Dietary Iron Controls Circadian Hepatic Glucose Metabolism Through Heme Synthesis

Diabetes 2015;64:1108–1119 | DOI: 10.2337/db14-0646

The circadian rhythm of the liver maintains glucose homeostasis, and disruption of this rhythm is associated with type 2 diabetes. Feeding is one factor that sets the circadian clock in peripheral tissues, but relatively little is known about the role of specific dietary components in that regard. We assessed the effects of dietary iron on circadian gluconeogenesis. Dietary iron affects circadian glucose metabolism through heme-mediated regulation of the interaction of nuclear receptor subfamily 1 group d member 1 (Rev-Erbα) with its cosuppressor nuclear receptor corepressor 1 (NCOR). Loss of regulated heme synthesis was achieved by aminolevulinic acid (ALA) treatment of mice or cultured cells to bypass the rate-limiting enzyme in hepatic heme synthesis, ALA synthase 1 (ALAS1). ALA treatment abolishes differences in hepatic glucose production and in the expression of gluconeogenic enzymes seen with variation of dietary iron. The differences among diets are also lost with inhibition of heme synthesis with isonicotinylhydrazine. Dietary iron modulates levels of peroxisome proliferator–activated receptor γ coactivator 1α (PGC-1α), a transcriptional activator of ALAS1, to affect hepatic heme. Treatment of mice with the antioxidant *N*-acetylcysteine diminishes PGC-1α variation observed among the iron diets, suggesting that iron is acting through reactive oxygen species signaling.

Circadian rhythms are endogenous cycles of behavioral and physiological processes that are set by external signals called zeitgebers. Light is the zeitgeber for the central clock of the suprachiasmatic nucleus (SCN) that controls circadian movement, feeding behavior, and thermoregulation (1). These SCN-driven physiological factors contribute to the synchronization of clocks in peripheral tissues, but peripheral clocks also entrain to non-SCN zeitgebers. Notably, the liver is entrained to food intake and can become dyssynchronous from the SCN (2). Both circulating glucose and hepatic gluconeogenesis are regulated by circadian factors, leading to the hypothesis that dyssynchrony between central and peripheral clocks may contribute to the observed association between metabolic dysregulation and altered sleep rhythms (3).

The precise contribution of specific nutrients to setting the hepatic clock is incompletely understood. One micronutrient, iron, has significant effects on metabolism. Iron affects metabolic regulation through multiple mechanisms including effects on AMP-dependent kinase, fuel preference, insulin secretion, and regulation of the insulin-sensitizing adipokine adiponectin (3,4). Iron overload and excess dietary iron are also significant risk factors for diabetes (5–7). Iron is a particularly attractive candidate for contributing to changes in circadian metabolism: not only is iron an essential component of several proteins involved with electron transport and metabolism, but also several circadian transcription factors bind heme. Heme, for example, is necessary for the formation of the complex of nuclear receptor subfamily 1 group d member 1 (Rev-Erbα) with nuclear receptor corepressor 1 (NCOR), part of the negative arm of the circadian transcriptional feedback loop (8,9). Heme has also been reported to bind the circadian proteins Clock and Per2, although the functional relevance of this binding is unknown and has been questioned (10–12).

To test the hypothesis that dietary iron intake may affect circadian metabolic rhythms, we fed mice chow with various iron concentrations, creating tissue iron levels

[1]Department of Biochemistry, University of Utah, Salt Lake City, UT
[2]Department of Internal Medicine, University of Utah, Salt Lake City, UT
[3]Veterans Administration Research Service, VA Salt Lake City Health Care System, Salt Lake City, UT

Corresponding author: Donald A. McClain, donald.mcclain@hsc.utah.edu.

Received 7 May 2014 and accepted 6 October 2014.

This article contains Supplementary Data online at http://diabetes.diabetesjournals.org/lookup/suppl/doi:10.2337/db14-0646/-/DC1.

See accompanying article, p. 1091.

within the range found from normal variation in human diets. We demonstrate that dietary iron content affects gluconeogenesis and circadian rhythm through modifying hepatic heme levels with concordant changes in Rev-Erbα binding to NCOR. Iron elicits these effects through peroxisome proliferator–activated receptor γ coactivator 1α (PGC-1α)–mediated regulation of the rate-limiting enzyme of heme synthesis in nonerythroid cells aminolevulinic acid synthase 1 (ALAS1).

RESEARCH DESIGN AND METHODS

Animal Studies

Three-month-old male C57BL/6J mice were fed diets of 35 mg/kg (TD.10211), 500 mg/kg (TD.10212), or 2 g/kg carbonyl iron (TD.10324) (Harlan Teklad, Madison, WI; by weight, 17.7% protein, 60.1% carbohydrate, and 7.2% fat) for 6 weeks before in vivo physiological testing and 9 weeks before sacrifice. The 35-mg/kg diet is derived from the AIN93G diet, the 500-mg/kg diet is based on animal facility diets that range from 200 to 500 mg/kg, and the 2-g/kg diet was selected due to the modest twofold increase in liver iron stores, which is within the fourfold range seen in hepatic iron among humans without iron-related pathology (13). The effects of heme iron were also assessed; heme iron diet was provided to the mice as previously described by Ijssennagger et al. (14).

The animals were maintained on a 12-h light/dark cycle. Treatment of mice with 2 mg/mL aminolevulinic acid (ALA) (15) (#A167; Frontier Scientific), 1 mg/mL isonicotinylhydrazine (INH) (16) (#I3377; Sigma-Aldrich), or 6.5 mg/mL *N*-acetylcysteine (NAC) (17) (#A9165; Sigma-Aldrich) in their drinking water and adjusted to pH 7. Water intake was monitored to ensure there were no variations. ALA treatment began after 6 weeks on diet and continued for 3 weeks concurrent with continued diet. Mice were treated with NAC or INH for 10 days after 8 weeks on diet. In the case of NAC treatment, water was changed every 2 days to prevent oxidation. Prior to glucose tolerance test (GTT), mice were fasted for 6 h and then challenged with 1 mg glucose/g body weight through i.p. injection. For pyruvate tolerance test (PTT), ad libitum–fed mice were challenged with 2 mg pyruvate/g body weight through i.p. injection. To monitor movement, food intake, and respiration, mice were housed in the Comprehensive Laboratory Animal Monitoring system for 7 days with the first 3 days as an acclimatization period (Comprehensive Lab Animal Monitoring System; Columbus Instruments, Columbus, OH). For transcriptional studies, mice were harvested at 4-h time points at zeitgeber time (ZT) 2, ZT6, ZT10, ZT14, ZT18, and ZT22. Procedures were approved by the Institutional Animal Care and Use Committee of the University of Utah and the Veterans Administration.

Blood and Serum Measurements

Hematocrit and hemoglobin were measured by Vetscan hm5, while insulin and glucagon were measured by ELISA (EMD Millipore Corp., Billerica, MA; Phoenix Pharmaceuticals Inc., Burlingame, CA).

Cell Culture

HepG2 cells (American Type Culture Collection) were maintained in DMEM/Nutrient Mixture F-12 supplemented with 10% FBS and 0.1% primocin. The cells were plated on six-well plates overnight and then treated with ferric ammonium citrate (FAC; 10 μmol), ALA (100 μg/mL), INH (5 mmol), or a PBS no-treatment control for 12 h. After the drug or iron treatment, the plate was synchronized with a 100 nmol dexamethasone shock for 1 h; after this time, the media was removed, the cells washed with PBS, and DMEM/Nutrient Mixture F-12 with treatment was replaced. Cells were harvested at 4-h intervals from the time of shock. Knockdown of PGC-1α was accomplished by PGC-1α small interfering RNA (siRNA) from Santa Cruz Biotechnology (sc-38885), following the company's general protocol with control siRNA (sc-37007) and transfection reagent (sc-29528).

RT-PCR

RNA was isolated from liver samples using RNeasy (Qiagen) and measured by Nanodrop (EPOCH). cDNA was synthesized with the SuperScript III First-Strand Synthesis System (Invitrogen). Measurement of relative abundance was performed by real-time PCR analysis using the Power SYBR Green Master Mix (Applied Biosciences) on a QuantStudio 12 K Flex System with 384-well block. The standard curve was prepared by serial dilution of pooled cDNA from each sample using five $\log_{10}$ standards. Rpl13 and cyB were selected as reference genes because they do not fluctuate temporally or vary with dietary iron (data not shown). Quantities were calculated by QuantStudio expression suite software based on the standard curve. Primers were designed using the National Institutes of Health–facilitated Mouse Primer Depot (http://mouseprimerdepot.nci.nih.gov/).

Western Blotting

Antibodies used included Rev-Erbα (Santa Cruz Biotechnology), NCOR, β-actin (Cell Signaling Technology), and PGC-1α (Abcam). The Criterion running and transfer system with precast gels was used (Bio-Rad).

Heme Measurement

Heme was measured by pyridine hemochrome spectrophotometric assay and high-performance liquid chromatography (HPLC) (18). In the pyridine hemochrome assay, heme was extracted from tissue samples with 500 mmol NaOH and pyridine added to 40%. Wave scans measured from 450 to 620 nm using an Ultrospec 3000 spectrophotometer, after addition of 1 mol potassium ferricyanide and sodium dithionite crystals. Data were analyzed using published extinction coefficients. For reverse-phase HPLC measurements, liver samples were homogenized in acidified acetone, filtered (0.45 μmol), and HPLC measurements performed on a Waters 2690 pump with C18 reverse-phase column (39 × 300 mm Waters μBondapak) and C18 precolumn (Waters 2690; Waters 996 photodiode array detector). Samples (0.125 μL) were eluted over a 15-min period using a linear gradient of 60% buffer A (0.56 mmol $NH_4H_2PO_4$ [pH 7]) to 100% methanol.

Iron Measurement

Equal amounts of liver lysate were digested with metal-free nitric acid for 12 h at 95°C (Optima; PerkinElmer, Boston, MA). Samples were centrifuged at 12,000 × *g* for 20 min and diluted with nanopure water (18 megaohm). Metal content was measured by inductively coupled plasma optical emission spectroscopy (Optima 3100XL; PerkinElmer), while nonheme iron measurements were performed by colorimetric assay (19). Standard curves were made from 1 mg Fe/mL solution (PFE1KN100; Fisher).

Iron Absorption and Transferrin Saturation

The iron absorption protocol used was previously described in Ajioka et al. (20). Mice were fasted overnight, and $^{59}FeCl_3$ was administered (200 μCi/kg body weight) by gavage. After 24 h, the mice were killed, the gastrointestinal tract harvested, and the radioactivity measured using a γ counter (PerkinElmer Instruments, Shelton, CT). Transferrin saturation was measured using an iron and iron binding capacity kit (Sigma-Aldrich).

Chromatin Immunoprecipitation

Chromatin immunoprecipitation (ChIP) studies were performed as previously described (4) using the Simple ChIP kit with company modifications for tissue samples (Cell Signaling Technology). Liver samples were homogenized in bead mill tubes with 1.44-mm ceramic beads and then cross-linked for 20 min with 1% formaldehyde; the cross linking was stopped with glycine, and the lysates were sonicated three times for 20 s using a sonic dismembrator (Fisher Scientific). Lysates were precleared, and A/G agarose beads were blocked with salmon sperm and BSA A/G (Millipore). NCOR, IgG, or histone H3 antibody (#5948, #2729, and #4620; Cell Signaling Technology) was applied for 1 h at room temperature. DNA was released from protein–DNA complexes by proteinase K digestion and quantified by real-time PCR for the enrichment at the PEPCK and glucose-6-phosphatase (G6Pase) promoter as well as using GAPDH and the PEPCK gene as negative controls to ensure appropriate sheering using the Power SYBR Green Master Mix (Applied Biosciences) (8). Occupancy was quantified to standard control and normalized to input control.

Coimmunoprecipitation

Liver protein lysates isolated in a standard HEPES lysis buffer were precleared with Protein A/G PLUS-Agarose beads (Santa Cruz Biotechnology). Rev-Erbα antibody (Santa Cruz Biotechnology) or a negative control IgG (Cell Signaling Technology) in 1× PBS was incubated with end-over-end mixing for 4 h at 4°C with Protein A/G PLUS-Agarose beads. The beads were washed five times with PBS buffer (100 mmol/L sodium phosphate and 150 mmol/L NaCl [pH 7.2] with 1 mmol/L $CaCl_2$ + 1 mmol/L $MgCl_2$). The protein lysate samples were then incubated with the beads overnight. Following protein incubation the beads were washed with PBS buffer (100 mmol/L sodium phosphate and 150 mmol/L NaCl [pH 7.2] with 1 mmol/L $CaCl_2$ + 1 mmol/L $MgCl_2$), and then samples were eluted with sample loading buffer.

Metabolite Measurement

This procedure was done as previously described (21). Briefly, 20 mg of freeze-clamped tissue was homogenized in bead mill tubes containing 500 μL of cold 90% MeOH containing internal standards. After a 20,000 × *g* centrifugation, the supernatant was collected, and the pellet was extracted again with cold 60% MeOH solution. The supernatants were combined and vacuum dried. Samples were reconstituted with 48 μL of 10 mmol/L sodium phosphate buffer (pH 7) followed by 2 μL of 2-vinylpyridine, and after 30 min at room temperature, 50 μL of 20 mmol/L ammonium formate buffer (pH 9.2) containing 7.5 mmol/L *N*-butylamine was added. After centrifuging at 20,000 × *g* for 5 min, 20 μL of sample was injected into Phenomenex (Torrance, CA) Gemini-NX C18 (150 × 3 mm; 3 μm particle size, 110 A pore size). Data were normalized to weight and internal standard.

Statistics

Statistics were done using JMP Pro statistical package and a two-tailed ANOVA with a Tukey-Kramer post hoc analysis to determine differences among multiple groups; these values are listed in the Supplementary Data. Results are presented as the mean ± SEM.

RESULTS

Dietary Iron Affects Circadian Glucose Metabolism

C57BL/6J male mice were fed high (H; 2 g iron/kg chow), high-normal (HN; 500 mg iron/kg chow), or low-normal (LN; 35 mg iron/kg chow) iron diets for 6 weeks. These levels of dietary iron are not so extreme as to cause neuropathy and allowed for normal hemoglobin concentrations and red blood cell volumes (hematocrit) to be maintained, but resulted in differences in blood transferrin saturation and gut iron absorption (Table 1) (22). In the liver, increasing dietary iron led to significant

Table 1—Physiologic parameters in mice fed diets containing different levels of iron

Variables	LN	HN	H
Hemoglobin (g/dL)	16.4 ± 0.5	15.6 ± 1.4	16.7 ± 1.7
Hematocrit (%)	47.9 ± 1.6	45.3 ± 3.4	47.6 ± 4.0
Insulin (ng/mL)	1.73 ± 0.65	1.52 ± 0.45	2.15 ± 0.38
Glucagon (pg/mL)	67.1 ± 5.5	60.4 ± 5.5	78.1 ± 8.7
Body weight‡ (g)	29.89 ± 0.27**	28.09 ± 0.25	28.65 ± 0.176
Total liver iron§ (μg/g wet weight)	158.1 ± 21.4*	239.4 ± 42.5	583.3 ± 79.3**
Transferin saturation (%)	44.1 ± 4.1	45.6 ± 4.9	58.5 ± 3.1*
Available ^{59}Fe absorption (%)	41.3 ± 4.2**	22.4 ± 3.1	8.8 ± 1.5*

*$P \leq 0.05$, **$P \leq 0.01$, by two-tailed ANOVA with Tukey post hoc analysis compared with HN. ‡N = 72/group. §Measured by inductively coupled plasma MS.

increases in nonheme iron and total iron, decreased transferrin receptor, and increased hepcidin transcripts (Table 1 and Supplementary Fig. 1). These changes are consistent with our previously published observation that liver ferritin protein levels increase in H diets (21).

Changes in dietary iron also resulted in differences in glucose homeostasis. The area under the glucose curve (AUCg) during GTT significantly varied with dietary iron at ZT0 (lights on) and ZT12 (lights off). Within diets, the AUCg varied significantly with time of day, as has been reported previously (23) (Fig. 1*A*). Fasting glucose values also differed among the dietary groups at ZT18 (Fig. 1*B*). To elucidate the mechanism behind these differences in glucose, we first measured ad libitum circulating insulin levels and saw no variation that would explain the changes (Table 1 and Supplementary Fig. 2*A*). We next assessed gluconeogenesis because it is a major contributor to serum glucose concentrations, and its dysregulation is seen early in diabetes. We have previously reported that high dietary iron significantly decreases gluconeogenesis as measured by using [U-$^{13}C_6$]-D-glucose (21). We validated these data by PTT performed at ZT12 when mice normally begin feeding and downregulate gluconeogenesis (Fig. 1*C* and *D*). Mice fed the LN diet exhibited higher levels of blood glucose in response to pyruvate injection compared with mice on the HN or H diets. Variations in glucagon did not account for these differences (Table 1). The LN-fed mice weighed 1.8 and 1.2 g more than the HN- and H-fed mice, respectively, although weight and AUCg were not significantly correlated across all individuals (Table 1; $P = 0.3944$, not shown).

We next assessed the transcript levels of gluconeogenic enzyme in the livers of the mice on the different iron diets. Consistent with the AUCg after pyruvate tolerance testing, the mRNA levels of PEPCK exhibited a significantly greater peak in mice on the LN diet when compared with the H- and HN-fed mice (Fig. 1*E*). G6Pase peak levels trended higher in the LN compared with the H group (Fig. 1*F*). Feeding behavior did not differ significantly (Supplementary Fig. 2*B*).

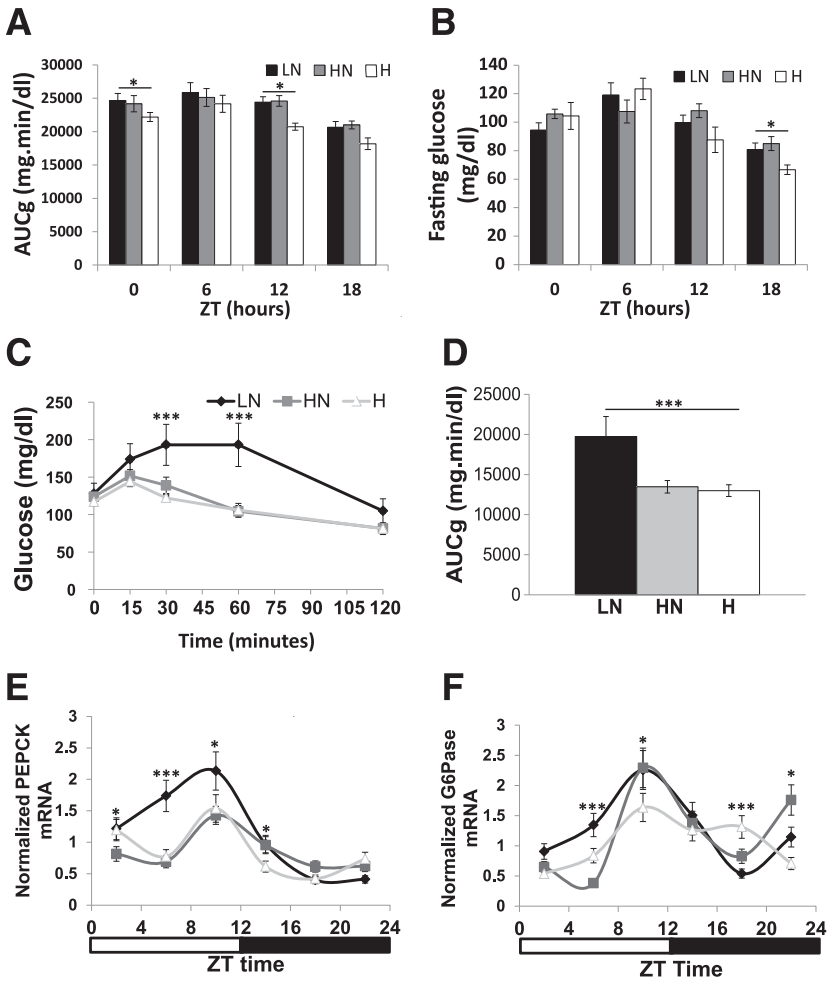

Figure 1—Dietary iron decreases parameters of glucose homeostasis and gluconeogenic transcription. *A*: AUCg for GTTs performed at various time points after a 6-h fast (n = 10–16). *B*: Fasting blood glucose levels obtained after 6-h fast throughout circade (n = 10–16). Ad libitum PTT (*C*) and the corresponding AUCg (*D*) at ZT12 (n = 11–16). Liver PEPCK (*E*) and G6Pase mRNA (n = 6) (*F*) as determined by RT-PCR normalized to cyB and Rpl13, housekeeping transcripts that did not display circadian variation (n = 6). *$P < 0.05$; ***$P < 0.001$.

Iron Alters Rev-Erbα Repressor Complex Formation and Activity

Because the parameters of glucose homeostasis exhibited temporal fluctuations that were dependent on dietary iron content, we next examined circadian regulatory factors that are associated with iron. Rev-Erbα is a member of the circadian regulon that directly inhibits PEPCK and G6Pase expression. This repressive activity requires heme for Rev-Erbα to bind NCOR to form the repressor complex (8). We assessed complex formation at ZT14, a time when circadian repression of gluconeogenic enzyme expression is beginning to manifest, by performing an immunoprecipitation (IP) of Rev-Erbα followed by immunoblotting for NCOR. We observed a direct correlation of complex formation with increased dietary iron (Fig. 2*A* and *B*), consistent with the observed decreases in gluconeogenesis and levels of gluconeogenic enzyme transcripts with higher dietary iron. Complex formation correlated with occupancy at ZT14 of the PEPCK and G6Pase promoters by NCOR, as revealed by ChIP (Fig. 2*C* and *D*). We did not observe variations in NCOR and Rev-Erbα transcript or protein between the diets at ZT14 (Supplementary Fig. 3).

Dietary Iron Alters Heme Levels and Temporal Expression of Enzymes Involved in Heme Synthesis and Degradation

The heme dependence of Rev-Erbα/NCOR repressor complex formation prompted us to measure hepatic heme levels. Livers were perfused with PBS to remove red blood cells, and total heme levels were assessed by HPLC (Fig. 3*A* and Supplementary Fig. 4*A*). A pyridine hemochromagen assay was performed to determine levels of heme B, the form that binds Rev-Erbα (Fig. 3*B* and Supplementary Fig. 4*B*) (9). In both assays, heme was highest in the H-fed mice at ZT12, which was the time at which we observed a rise in Rev-Erbα/NCOR complex formation (Fig. 2*A* and *B*). Conversely, at ZT0, heme levels were highest in the LN-fed mice (Supplementary Fig. 4*A* and *B*). The net result of these changes is that heme B levels show higher temporal variation in mice fed higher iron diets, as reflected in the ZT12/ZT0 ratios (LN = 0.778; HN = 1.69; and H = 3.02). Peak transcript levels of ALAS1 (Fig. 3*C*) increase with increased heme at ZT10, and heme oxygenase 1, an enzyme necessary for heme catabolism, showed a similar trend with dietary iron at ZT18 (Supplementary Fig. 4*C*). When mice were fed high dietary heme, we also saw similar results in PTT, gluconeogenic enzyme transcripts, and heme levels (Supplementary Fig. 5).

If ALAS1-mediated changes in heme levels are driving the changes in Rev-Erbα/NCOR association, we hypothesized that bypassing ALAS1 should increase heme levels and abrogate the effects of dietary iron on gluconeogenesis. Inhibiting heme synthesis should decrease heme levels, likewise limiting the effects of dietary iron. Treatment of mice with the product of ALAS1, ALA has been shown to increase heme levels in the liver and erythrocytes (15). Mice were therefore fed the LN, HN, and H iron diets for 6 weeks and concurrently treated with 2 mg/mL ALA in their drinking water for the final 3 weeks. At the end of this period, we determined heme levels in perfused liver by HPLC. Heme levels increased in all three diets (Fig.

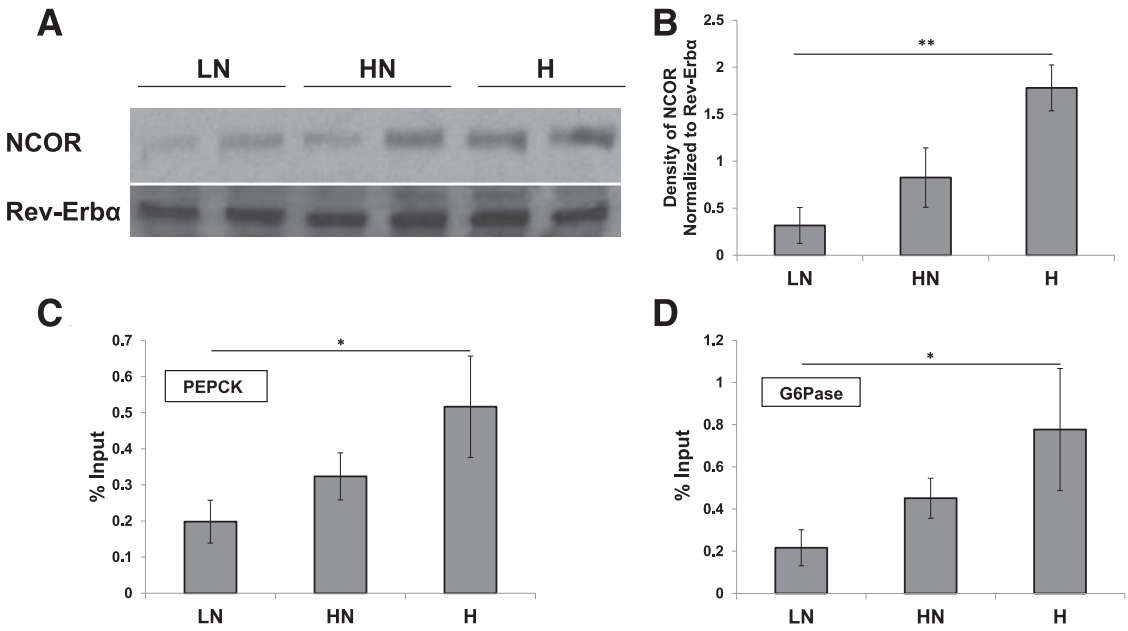

Figure 2—Dietary iron affects the formation of the Rev-Erbα repressor complex and its activity. Western blot of Rev-Erbα IP extracts blotted for NCOR and Rev-Erbα at ZT14 (*A*) and quantification of these blots ($n = 6$) (*B*). ChIP of NCOR to the PEPCK ($n = 4$) (*C*) and G6Pase promoter determined by RT-PCR normalized to input at ZT14 ($n = 4$) (*D*). Values are represented as percent input, which is calculated by dividing the threshold cycle value of the DNA recovered from each experimental IP by the threshold cycle of adjusted input (the initial input was 2%) and multiplying by 100. IgG control was subtracted out as baseline. *$P < 0.05$; **$P < 0.01$.

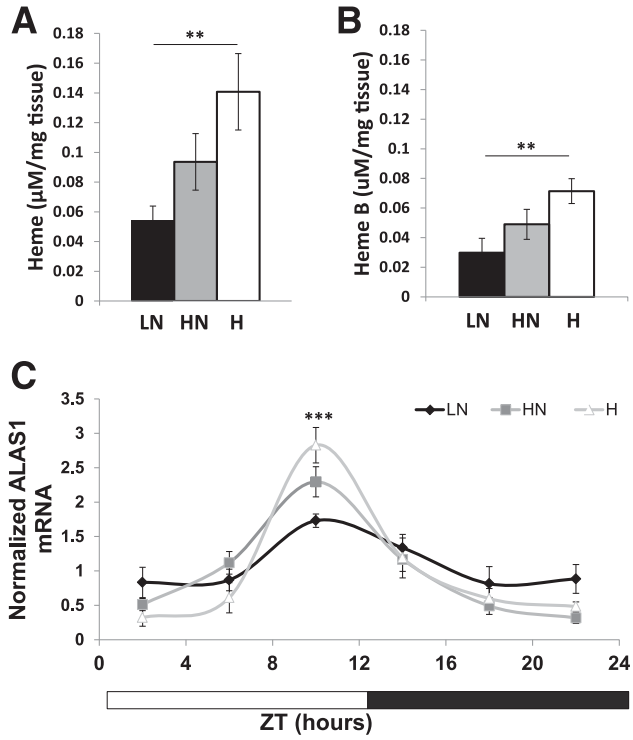

Figure 3—Hepatic heme synthesis and steady-state levels are altered with dietary iron. *A*: Total heme levels as measured by HPLC at ZT12 (n = 6). *B*: Heme B levels as measured by hemochromagen pyridine assay at ZT12 (n = 12). *C*: ALAS1 transcripts determined by RT-PCR normalized to cyB and Rpl13 (n = 6). $^{**}P < 0.01$; $^{***}P < 0.001$.

4*A*). Heme B levels showed a similar trend (Supplementary Fig. 4*D*). We performed PTTs on the ALA-treated and control mice at ZT12; ALA treatment abolished differences among the LN-, HN-, and H-fed mice (Fig. 4*B*). ALA treatment also diminished the differences in PEPCK and G6Pase mRNA levels observed in the control mice with the various iron diets (Fig. 4*C* and *D*). In general, the effect of ALA treatment was to decrease the PTT-AUCg and transcript levels in the LN mice toward the levels seen in the mice on the higher iron diets. Furthermore, IP of Rev-Erbα in ALA-treated and control livers showed increased NCOR coprecipitation with ALA treatment (Fig. 4*E* and *F*).

INH inhibits heme synthesis by decreasing pyridoxine, a cofactor for ALAS1. Mice were fed the iron diets for 8 weeks and then treated with INH in their drinking water for 10 days while continuing the iron diets. PTT was performed after 5 days of INH treatment, and tissues were harvested after 10 days. The results were the converse of those observed on ALA: the effect of INH was to increase the lower AUCg seen in the HN and H diets to a level resembling that observed in the mice on the LN diet (Fig. 4*H*). Similar effects were noted for PEPCK and G6Pase transcript levels (Fig. 4*I* and *J*). The INH treatment also decreased Rev-Erbα/NCOR complex formation in all of the iron diets, with the greatest relative effect seen in the H group (Fig. 4*K* and *L*).

Dietary Iron Alters Gluconeogenesis Cell Autonomously in a Human Hepatoma Model

To determine if dietary iron affects hepatocyte glucose production in a cell-autonomous manner as opposed to exerting more indirect (e.g., hormonal) effects, we treated HepG2 cells with FAC. Cells were grown for 12 h in control DMEM or DMEM with 10 μmol FAC, with or without treatment of ALA or INH. We then set a circadian rhythm in the cells with dexamethasone shock (24). The results were concordant with in vivo results. At the peak expression of PEPCK and G6Pase, non–iron-treated cells exhibited a greater PEPCK and G6Pase expression compared with the FAC-treated cells (Fig. 5*A* and *B*). Treatment of cells with the iron chelator deferoxamine ablated these rhythms in PEPCK and G6Pase (Supplementary Fig. 6). ALA treatment brings PEPCK and G6Pase transcript levels down in non–iron-treated cells, close to those observed in the FAC-treated cells (Fig. 5*A* and *B*, right panels). Conversely, INH increases transcript levels in the FAC-treated cells, close to those observed in non–iron-treated cells (Fig. 5*A* and *B*, left panels). During the peak times, we also assessed NCOR association with Rev-Erbα through a coprecipitation and were able to recapitulate the trends observed in the animals: FAC treatment increased association of NCOR and Rev-Erbα (Fig. 5*C* and *D*, middle panel). ALA treatment increased complex formation to levels seen in the FAC-treated cells, while INH treatment decreased association to levels seen in the non–iron-treated cells (Fig. 5*C* and *D*, left and right panels, respectively).

Variations in Heme Synthesis Are Due to Differences in PGC-1α Expression Related to Altered Oxidative Signaling in Mice Fed the Various Iron Diets

PGC-1α regulates ALAS1 transcription (25), leading us to explore its possible regulation by iron to explain the differences in heme synthesis among the iron diets. In mice, both PGC-1α transcript and protein levels increased with increasing dietary iron (Fig. 6*A*–*C*). In HepG2 cells, partial silencing of PGC-1α by siRNA treatment (Fig. 6*D*) ablated the differences in ALAS1, PEPCK, and G6Pase that occurred with FAC treatment (Fig. 6*E*–*G*).

PGC-1α is upregulated by reactive oxygen species (ROS) (26,27), and iron is known to create ROS through fenton chemistry. Therefore, we explored oxidative signaling as a mechanism through which dietary iron upregulates PGC-1α. Cellular oxidative markers differed temporally among the diets, with lower glutathione (GSH) levels (Fig. 7*A*) and NADPH/NADP+ ratios (Fig. 7*B*) in the H-fed mice, as well as the transcripts of enzymes involved in the oxidative response such as superoxide dismutase 1 (Supplementary Fig. 7). To blunt differences in oxidant levels among mice on the iron diets, we treated them with the antioxidant NAC. Differences observed in fasting glucose observed at ZT12 among the mice on LN, HN, and H diets were reversed by NAC treatment: NAC had no effect on fasting glucose in the LN mice but increased glucose in mice on the HN diet and even more so in mice on the H diet. The livers of the

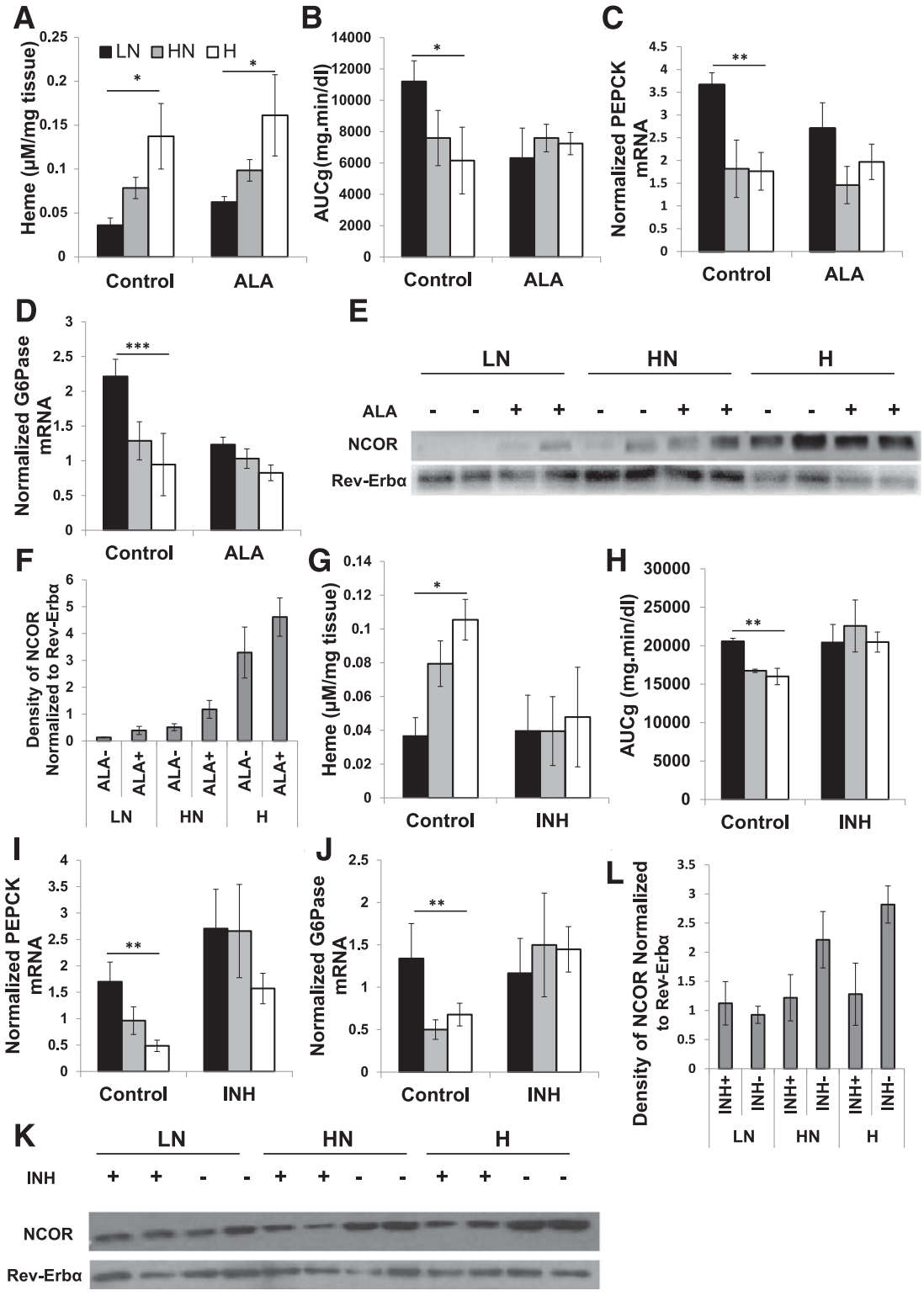

Figure 4— Drug-induced increase of heme ablates variations in heme, Rev-Erbα/NCOR complex formation, and gluconeogenesis observed among the various diets. *A*: Heme levels as measured by HPLC with ALA treatment and control (n = 6–12). AUCg from ZT12 PTT (n = 6) (*B*), PEPCK (n = 9) (*C*), and G6Pase mRNA transcripts in ALA-treated and control mice normalized to Rpl13 and cyB (n = 9) (*D*). Western blot of Rev-Erbα IP extracts blotted for NCOR and Rev-Erbα (*E*) and quantification of the density of the NCOR blot normalized to the Rev-Erbα density (n = 4–6) (*F*). *G*: Heme levels as measured by HPLC with INH-treated and control mice (n = 3). AUCg for ZT12 PTT (n = 5–8) (*H*), PEPCK (n = 5–8) (*I*), and G6Pase transcript levels as measured by RT PCR normalized to Rpl13 and cyclophilin in INH-treated and control mice (n = 5–8) (*J*). Western blot for Rev-Erbα/NCOR coimmunoprecipitation extracts blotted for Rev-Erbα and NCOR (n = 6) (*K*) and quantified density of NCOR bands normalized to Rev-Erbα density (n = 6) (*L*). *P < 0.05; **P < 0.01; ***P < 0.001.

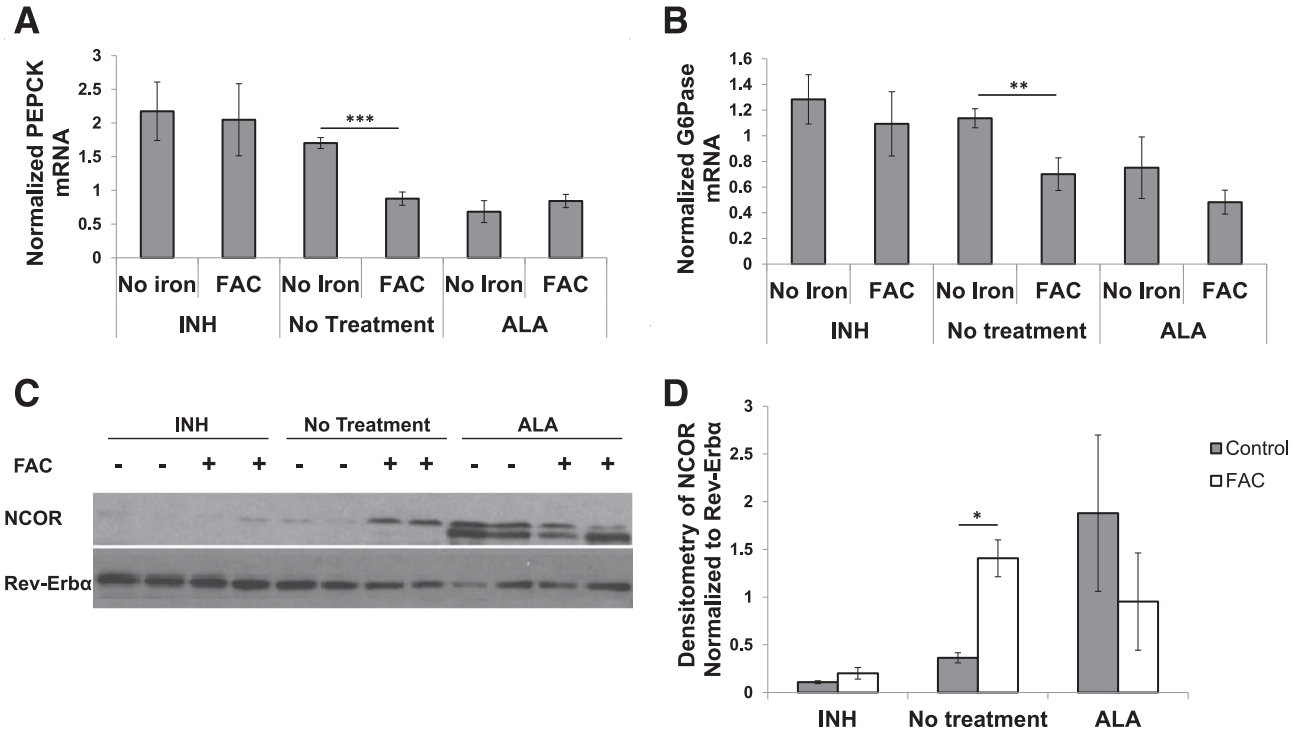

Figure 5—Treatment of HepG2 cells with FAC, ALA, or INH recapitulates mouse results. PEPCK (n = 12–24) (*A*) and G6Pase (*B*) transcript levels as measured by RT-PCR for control and FAC cells with no drug treatment or ALA or INH treatment (n = 12–24). Western blot of Rev-Erbα IP cell extract blotted for NCOR and Rev-Erbα (*C*) and quantification of the density of the NCOR band as normalized to Rev-Erbα (n = 3) (*D*). $^*P < 0.05$; $^{**}P < 0.01$; $^{***}P < 0.001$.

mice were harvested at ZT12. NAC treatment abolished differences in PGC-1α, PEPCK, G6Pase, ALAS1, GSH, and NADPH/NADP+ ratios between the diets (Fig. 7*D–I*).

DISCUSSION

Iron is a risk factor for several parameters of metabolic syndrome. For example, a high serum ferritin level, a marker of tissue iron stores, is associated with insulin resistance and type 2 diabetes (28). This relationship between iron and metabolic syndrome highlights the role of iron as both a structural component of proteins involved in bioenergetics and a cellular regulator of metabolic pathways such as AMPK activity (4,21). We show in this study yet another role of iron in metabolism, namely that dietary iron affects the circadian rhythm of hepatic gluconeogenesis by altering heme synthesis that in turn affects the activity of a key component of the circadian machinery, Rev-Erbα (Fig. 8).

Besides being a crucial component of the circadian clock, Rev-Erbα regulates many aspects of glucose and lipid metabolism, including acting as a negative transcriptional regulator of gluconeogenic enzymes. Decreased Rev-Erbα expression is associated with hyperglycemia and obesity in mice and humans (8,29–31). Previous work has shown that Rev-Erbα activity is dependent on the formation of a repressor complex with NCOR, which requires heme (8). We verified the dependence of this complex formation on heme availability and further showed that liver heme levels temporally fluctuate and vary with dietary iron. The results demonstrate that heme availability is altered by dietary iron and is a regulating factor in the circadian rhythm of hepatic gluconeogenesis. While heme is known to be required for Rev-Erbα/NCOR complex formation, the observations that heme availability is limiting for that process in normal physiologic circumstances has not been previously shown.

The changes in heme levels observed with increased dietary iron are not due to limiting amounts of iron for metalation of heme but rather by the regulation of heme synthesis by ALAS1. This is revealed by the facts that bypassing ALAS1 with ALA or inhibiting heme synthesis by INH abrogated the effects of dietary iron. If iron itself were limiting in the LN diet, for example, ALA would not be able to increase heme-dependent formation of the Rev-Erbα/NCOR complex in mice on that diet. Furthermore, mice on the lower levels of dietary iron show no evidence of systemic iron deficiency (Table 1). These data are supported by recent studies in humans that show that treatment with ALA is able to reduce fasting blood glucose (32).

ALAS1 itself exhibits a circadian rhythm controlled by PGC-1α and its binding partners nuclear respiratory factor 1 or forkhead box 1 (FOXO1) (33). We confirmed the circadian rhythm of ALAS1 transcripts in the current study and show that the magnitude of its excursions is significantly

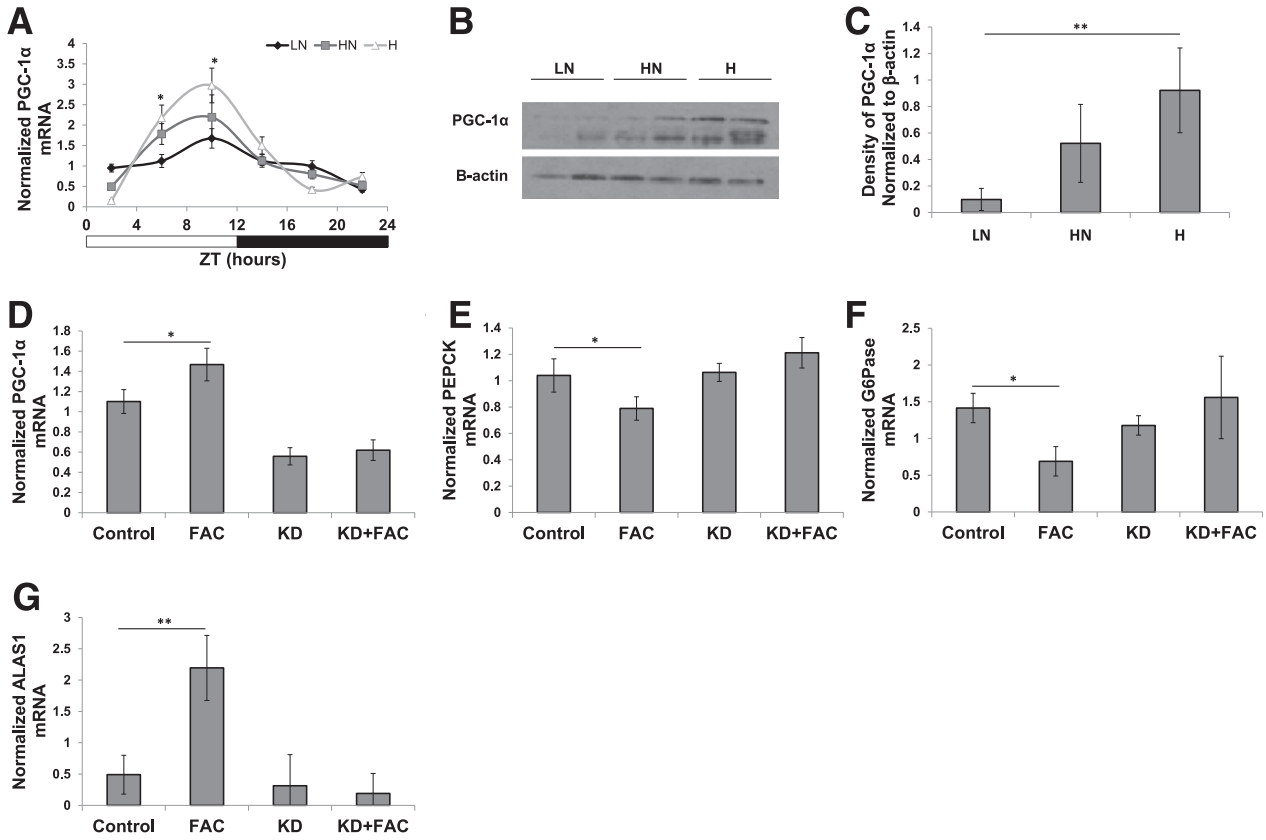

Figure 6—Increased dietary iron increases PGC-1α, and knockdown of PGC-1α abrogates differences between iron-treated and non-treated HepG2 cells. *A*: PGC-1α mRNA as measured by RT-PCR (n = 6, ZT6, P = 0.036; LN vs. H, P = 0.0272; ZT10, P = 0.0495; LN vs. H, P = 0.0472). Western blot of liver extracts blotted for PGC-1α at ZT10 (*B*) and density of PGC-1α band normalized to β-actin (*C*) (n = 6, P = 0.0092; LN vs. H, P = 0.0079; HN vs. H, P = 0.0734). Verification of PGC-1α knockdown by RT-PCR (n = 6, control vs. FAC, P = 0.0167) (*D*), PEPCK (n = 6, control vs. FAC, P = 0.048) (*E*), G6Pase (n = 6, control vs. FAC, P = 0.037) (*F*), and ALAS1 transcript levels in PGC-1α knockdown normalized to Rpl13 (n = 6) (*G*). KD, knockdown. *P < 0.05; **P < 0.01.

altered by dietary iron. The regulation of ALAS1 is not mediated directly by iron responsive proteins, as it is for the erythroid form of the enzyme ALAS2 (34). Rather, iron drives increased PGC-1α expression that in turn transcriptionally activates ALAS1. This was demonstrated by the fact that the effects of iron on ALAS1, PEPCK, and G6Pase were not seen after knockdown of PGC-1α in HepG2 cells. The circadian timing of these events in vivo corresponds to the feeding behavior of mice, which is crepuscular in a laboratory setting with peaks in food intake seen at ZT0 and ZT12. It is the food intake at ZT0 that is able to modulate the oxidative setting and synchronize the later peaks in heme synthesis.

PGC-1α is a transcriptional coactivator that is known to be involved in a number of diverse metabolic pathways including circadian rhythms, mitochondrial biogenesis, adaptive thermogenesis, and metabolism of both glucose and lipids (35,36). Dietary iron has been shown to alter the expression of PGC-1α: decreased protein levels are observed in the skeletal muscle of rats fed an iron-deficient diet, although the mechanism of this change was not determined (37). We demonstrate that iron regulation of PGC-1α occurs at least in part through oxidant-sensing pathways. Mice on the higher iron diets show evidence of changes in intracellular redox state as revealed by decreased GSH and decreased NADPH/NADP+ ratios. Treatment of mice with the antioxidant NAC eliminated the variation seen in PGC-1α, ALAS1, PEPCK, and G6Pase among the different iron diets. These data suggest that dietary iron is acting through ROS to exert effects upon heme synthesis and subsequently gluconeogenesis.

While we have observed significant effects of iron on the expression of gluconeogenic enzymes, the overall regulation of gluconeogenesis is controlled by numerous other hormonal, signaling, and transcription factors. Further complicating this intricate pathway is the fact that PGC-1α also regulates gluconeogenesis more directly, increasing transcription of PEPCK and G6Pase through coactivation of hepatic nuclear factor-4α, glucocorticoid receptor, and FOXO1 (38). Thus, the apparently paradoxical observation that PGC-1α increases in H-fed mice while PEPCK and G6Pase transcripts are decreased could be due to multiple promoter inputs from both AMPK and Rev-Erbα/NCOR or differences in PGC-1α binding partners. Furthermore, in previous studies, we have shown that iron alters FOXO1-dependent transcription and levels of

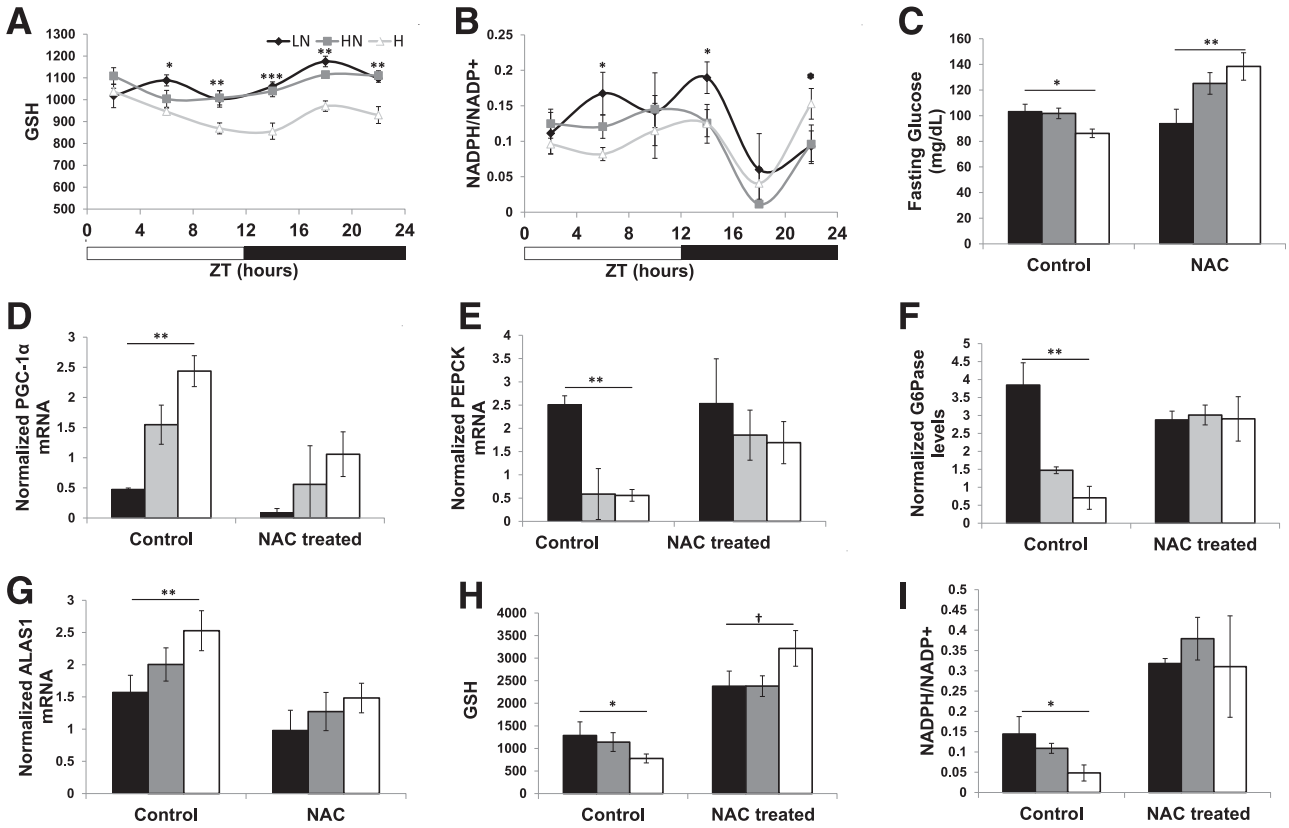

Figure 7—Dietary iron alters hepatocyte oxidant signaling and antioxidant treatment ablates differences in PGC-1α and gluconeogenic transcripts. GC MS/MS measurement of GSH (n = 6) (*A*) and NADPH/NADP+ (*B*) in freeze-clamped liver of mice on iron diets at various harvest times (n = 6). *C*: Fasting blood glucose measurements in control and NAC-treated mice (n = 5–10). Transcript levels of PGC-1α (n = 3–6) (*D*), PEPCK (n = 3–6) (*E*), G6Pase (n = 3–6) (*F*), and ALAS1 in NAC-treated and control mice (n = 3–6) (*G*). GC MS/MS measurement of GSH (n = 3–6) (*H*) and NADPH/NADP+ (*I*) in NAC-treated or control mice at ZT12 (n = 3–6). *P < 0.05; **P < 0.01; ***P < 0.001; †P = 0.147.

the FOXO1 acetylation (4). This system is also complicated by research that shows gluconeogenic signals regulate iron uptake, suggesting that iron metabolism and glucose homeostasis are tightly coupled processes (39).

Previous work on iron and metabolism has concentrated on pathologic iron overload. However, increased diabetes risk is seen even with modest levels of iron excess such as higher dietary iron intake (6,40). On the surface, this correlation of high iron with increased diabetes risk appears contradictory to our results of high iron being associated with improved glucose tolerance and hepatic glucose production. However, type 2 diabetes is a multifactorial disease, and the prodiabetic effects of iron on insulin production and adipokines may, over time, overwhelm other apparently antidiabetic effects such as those observed on hepatic gluconeogenesis (4,21,41). Furthermore, the increased magnitude of circadian variation in hepatic gluconeogenesis seen in the H-fed mice could be prodiabetic under certain circumstances. For example, in situations of nightshift work, sleep disturbance, or snacking during the night, all of which are associated with increased diabetes risk (42), it might be expected that individuals with higher iron would suffer greater dyssynchrony and disruption of normal metabolic regulation.

Besides its effects on ROS and heme availability, the effects of iron on metabolism are likely to be widespread and not explained by a single mechanism. The drosophila Rev-Erbα homolog E75 is regulated by nitric oxide (43), and transcript levels of nitric oxide synthase, the rate-limiting enzyme in nitric oxide synthesis, were increased with increasing dietary iron at certain time points (not shown). Further, the redox state of thiols within the heme-binding pocket of proteins such as Rev-Erbα also regulates heme binding (44).

Although our work has focused on hepatic gluconeogenesis in mammals, the effects of iron on circadian rhythms are also seen in plants (45) and insects (46), and they are manifest in multiple organ systems and tissues including the central clock of the SCN. Iron deficiency in mice, for example, alters thermoregulation, behavior, and monoamine metabolism and dopamine transporter expression in the central nervous system (47,48). Furthermore, knockdown of the drosophila homolog of ferritin in circadian neurons disrupts the molecular components of the central clock (46).

In summary, we have demonstrated that one mechanism through which dietary iron is able to regulate the core molecular clock in the liver is through regulation of

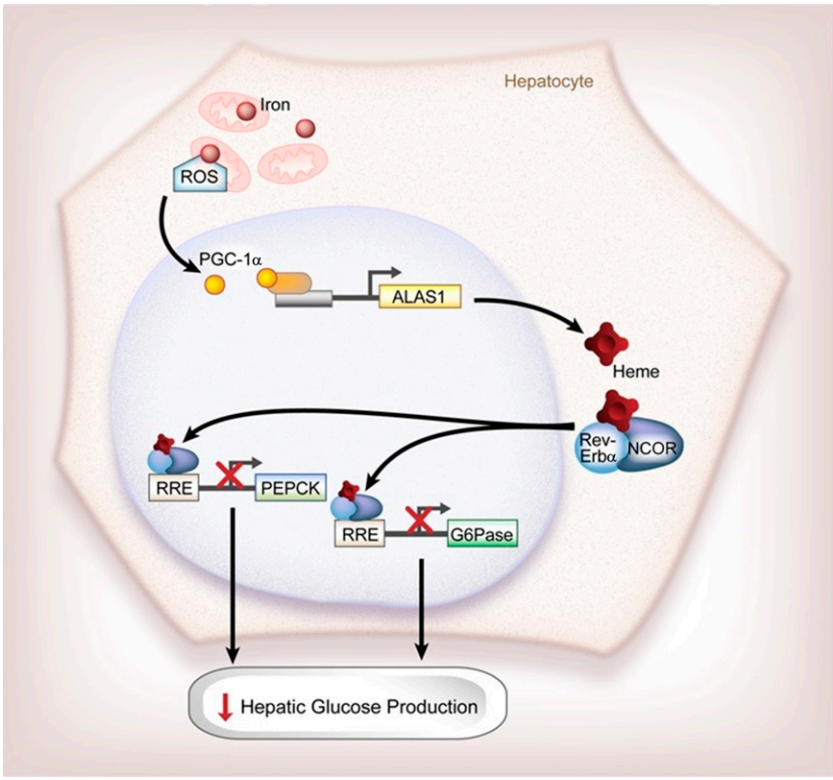

Figure 8—Schematic representation of the effects of dietary iron on circadian gluconeogenesis. Dietary iron alters the oxidative state of the cell to increase the transcription of PGC-1α, which then regulates heme synthesis. These changes in heme synthesis in turn increase the complex formation of Rev-Erbα and NCOR to inhibit the transcription of gluconeogenic enzymes PEPCK and G6Pase to decrease hepatic glucose production. RRE, Rev/Erb-responsive element.

heme synthesis. This novel role of iron provides another mechanism through which iron acts to regulate glucose metabolism. The studies suggest mechanisms that may underlie the interplay among iron, altered circadian rhythms, metabolic regulation, and diabetes risk.

Acknowledgments. The authors thank Diana Lim, IT project manager from the University of Utah Molecular Medicine Program, for assistance with the illustrations.

Funding. This work was supported by the Research Service of the Department of Veterans Affairs and the National Institutes of Health (1R01-DK-081842 to D.A.M. and 1T32-DK-091317 to J.A.S.).

Duality of Interest. No potential conflicts of interest relevant to this article were reported.

Author Contributions. J.A.S. conducted all experiments and wrote the manuscript, except the portions indicated below. T.C.M. aided with total iron measurement, heme measurement, and RT-PCR of INH-treated mice. Y.G. aided with coimmunoprecipitation of Rev-Erbα and NCOR in mice treated with ALA. S.F.J. helped with synchronization of HepG2 cells and circadian harvest of cells. R.C. aided with liver perfusion and performed HPLC heme measurement. J.C. performed metabolite measurements and wrote the corresponding RESEARCH DESIGN AND METHODS section. R.A. measured iron absorption and transferrin saturation. D.J. aided with liver perfusion, GTTs, PTTs, metabolic chamber housing, and tissue harvest. S.-h.L. aided with tissue harvest, liver perfusion, and GTTs. D.K. helped with RNA isolation, cDNA synthesis, and RT-PCR of cell culture. J.H. aided with PTTs and RT-PCR of initial gluconeogenic transcripts. D.A.M. oversaw experimental design, experiments, and data analysis and interpretation, in addition to writing the manuscript. D.A.M. is the guarantor of this work and, as such, had full access to all the data in the study and takes responsibility for the integrity of the data and the accuracy of the data analysis.

References

1. Buhr ED, Yoo SH, Takahashi JS. Temperature as a universal resetting cue for mammalian circadian oscillators. Science 2010;330:379–385
2. Stokkan KA, Yamazaki S, Tei H, Sakaki Y, Menaker M. Entrainment of the circadian clock in the liver by feeding. Science 2001;291:490–493
3. Huang J, Jones D, Luo B, et al. Iron overload and diabetes risk: a shift from glucose to Fatty Acid oxidation and increased hepatic glucose production in a mouse model of hereditary hemochromatosis. Diabetes 2011;60:80–87
4. Gabrielsen JS, Gao Y, Simcox JA, et al. Adipocyte iron regulates adiponectin and insulin sensitivity. J Clin Invest 2012;122:3529–3540
5. Simcox JA, McClain DA. Iron and diabetes risk. Cell Metab 2013;17:329–341
6. Bowers K, Yeung E, Williams MA, et al. A prospective study of prepregnancy dietary iron intake and risk for gestational diabetes mellitus. Diabetes Care 2011;34:1557–1563
7. Qiu C, Zhang C, Gelaye B, Enquobahrie DA, Frederick IO, Williams MA. Gestational diabetes mellitus in relation to maternal dietary heme iron and nonheme iron intake. Diabetes Care 2011;34:1564–1569
8. Yin L, Wu N, Curtin JC, et al. Rev-erbalpha, a heme sensor that coordinates metabolic and circadian pathways. Science 2007;318:1786–1789
9. Raghuram S, Stayrook KR, Huang P, et al. Identification of heme as the ligand for the orphan nuclear receptors REV-ERBalpha and REV-ERBbeta. Nat Struct Mol Biol 2007;14:1207–1213
10. Kaasik K, Lee CC. Reciprocal regulation of haem biosynthesis and the circadian clock in mammals. Nature 2004;430:467–471

11. Lukat-Rodgers GS, Correia C, Botuyan MV, Mer G, Rodgers KR. Heme-based sensing by the mammalian circadian protein CLOCK. Inorg Chem 2010;49:6349–6365
12. Airola MV, Du J, Dawson JH, Crane BR. Heme binding to the Mammalian circadian clock protein period 2 is nonspecific. Biochemistry 2010;49:4327–4338
13. Milman N, Graudal N, Hegnhøj J, Christoffersen P, Pedersen NS. Relationships among serum iron status markers, chemical and histochemical liver iron content in 117 patients with alcoholic and non-alcoholic hepatic disease. Hepatogastroenterology 1994;41:20–24
14. Ijssennagger N, de Wit N, Müller M, van der Meer R. Dietary heme-mediated PPARα activation does not affect the heme-induced epithelial hyperproliferation and hyperplasia in mouse colon. PLoS ONE 2012;7:e43260
15. Phillips JD, Jackson LK, Bunting M, et al. A mouse model of familial porphyria cutanea tarda. Proc Natl Acad Sci U S A 2001;98:259–264
16. Chalmers JG. The effect of isoniazid on the clearance of pyruvic and alpha-oxoglutaric acids in the urine of mice, meriones lybicus and rats. Br J Cancer 1965;19:430–432
17. Potts-Kant EN, Li Z, Tighe RM, et al. NAD(P)H:quinone oxidoreductase 1 protects lungs from oxidant-induced emphysema in mice. Free Radic Biol Med 2012;52:705–715
18. Sinclair PR, Gorman N, Jacobs JM. Measurement of heme concentration. Curr Protoc Toxicol 2001;Chapter 8:Unit 8.3
19. Torrance JD, Bothwell TH. A simple technique for measuring storage iron concentrations in formalinised liver samples. S Afr J Med Sci 1968;33:9–11
20. Ajioka RS, Levy JE, Andrews NC, Kushner JP. Regulation of iron absorption in Hfe mutant mice. Blood 2002;100:1465–1469
21. Huang J, Simcox J, Mitchell TC, et al. Iron regulates glucose homeostasis in liver and muscle via AMP-activated protein kinase in mice. FASEB J 2013;27:2845–2854
22. Sobotka TJ, Whittaker P, Sobotka JM, et al. Neurobehavioral dysfunctions associated with dietary iron overload. Physiol Behav 1996;59:213–219
23. Ben-Dyke R. Diurnal variation of oral glucose tolerance in volunteers and laboratory animals. Diabetologia 1971;7:156–159
24. Balsalobre A, Brown SA, Marcacci L, et al. Resetting of circadian time in peripheral tissues by glucocorticoid signaling. Science 2000;289:2344–2347
25. Estall JL, Ruas JL, Choi CS, et al. PGC-1alpha negatively regulates hepatic FGF21 expression by modulating the heme/Rev-Erb(alpha) axis. Proc Natl Acad Sci U S A 2009;106:22510–22515
26. Marmolino D, Manto M, Acquaviva F, et al. PGC-1alpha down-regulation affects the antioxidant response in Friedreich's ataxia. PLoS ONE 2010;5:e10025
27. Wu Z, Puigserver P, Andersson U, et al. Mechanisms controlling mitochondrial biogenesis and respiration through the thermogenic coactivator PGC-1. Cell 1999;98:115–124
28. Forouhi NG, Harding AH, Allison M, et al. Elevated serum ferritin levels predict new-onset type 2 diabetes: results from the EPIC-Norfolk prospective study. Diabetologia 2007;50:949–956
29. Goumidi L, Grechez A, Dumont J, et al. Impact of REV-ERB alpha gene polymorphisms on obesity phenotypes in adult and adolescent samples. Int J Obes (Lond) 2013;37:666–672
30. Delezie J, Dumont S, Dardente H, et al. The nuclear receptor REV-ERBalpha is required for the daily balance of carbohydrate and lipid metabolism. FASEB J 2012;26:3321–3335
31. Cho H, Zhao X, Hatori M, et al. Regulation of circadian behaviour and metabolism by REV-ERB-α and REV-ERB-β. Nature 2012;485:123–127
32. Higashikawa F, Noda M, Awaya T, Tanaka T, Sugiyama M. 5-aminolevulinic acid, a precursor of heme, reduces both fasting and postprandial glucose levels in mildly hyperglycemic subjects. Nutrition 2013;29:1030–1036
33. Handschin C, Lin J, Rhee J, et al. Nutritional regulation of hepatic heme biosynthesis and porphyria through PGC-1alpha. Cell 2005;122:505–515
34. Ajioka RS, Phillips JD, Kushner JP. Biosynthesis of heme in mammals. Biochim Biophys Acta 2006;1763:723–736
35. Liang H, Ward WF. PGC-1alpha: a key regulator of energy metabolism. Adv Physiol Educ 2006;30:145–151
36. Lin JD. Minireview: the PGC-1 coactivator networks: chromatin-remodeling and mitochondrial energy metabolism. Mol Endocrinol 2009;23:2–10
37. Han DH, Hancock CR, Jung SR, Higashida K, Kim SH, Holloszy JO. Deficiency of the mitochondrial electron transport chain in muscle does not cause insulin resistance. PLoS ONE 2011;6:e19739
38. Rhee J, Inoue Y, Yoon JC, et al. Regulation of hepatic fasting response by PPARgamma coactivator-1alpha (PGC-1): requirement for hepatocyte nuclear factor 4alpha in gluconeogenesis. Proc Natl Acad Sci U S A 2003;100:4012–4017
39. Vecchi C, Montosi G, Garuti C, et al. Gluconeogenic signals regulate iron homeostasis via hepcidin in mice. Gastroenterology 2014;146:1060–1069.e1063
40. Jiang R, Manson JE, Meigs JB, Ma J, Rifai N, Hu FB. Body iron stores in relation to risk of type 2 diabetes in apparently healthy women. JAMA 2004;291:711–717
41. Jouihan HACP, Cobine PA, Cooksey RC, et al. Iron-mediated inhibition of mitochondrial manganese uptake mediates mitochondrial dysfunction in a mouse model of hemochromatosis. Mol Med 2008;14:98–108
42. Hatori M, Vollmers C, Zarrinpar A, et al. Time-restricted feeding without reducing caloric intake prevents metabolic diseases in mice fed a high-fat diet. Cell Metab 2012;15:848–860
43. Cáceres L, Necakov AS, Schwartz C, Kimber S, Roberts IJ, Krause HM. Nitric oxide coordinates metabolism, growth, and development via the nuclear receptor E75. Genes Dev 2011;25:1476–1485
44. Gupta N, Ragsdale SW. Thiol-disulfide redox dependence of heme binding and heme ligand switching in nuclear hormone receptor rev-erbbeta. J Biol Chem 2011;286:4392–4403
45. Chen YY, Wang Y, Shin LJ, et al. Iron is involved in the maintenance of circadian period length in Arabidopsis. Plant Physiol 2013;161:1409–1420
46. Mandilaras K, Missirlis F. Genes for iron metabolism influence circadian rhythms in Drosophila melanogaster. Metallomics 2012;4:928–936
47. Bianco LE, Unger EL, Earley CJ, Beard JL. Iron deficiency alters the day-night variation in monoamine levels in mice. Chronobiol Int 2009;26:447–463
48. Youdim MB, Yehuda S, Ben-Uriah Y. Iron deficiency-induced circadian rhythm reversal of dopaminergic-mediated behaviours and thermoregulation in rats. Eur J Pharmacol 1981;74:295–301